NANO MICRO small

Supporting Information

for *Small,* DOI: 10.1002/smll.202107426

3d Metal Doping of Core@Shell Wüstite@ferrite Nanoparticles as a Promising Route toward Room Temperature Exchange Bias Magnets

Beatrice Muzzi, Martin Albino, Michele Petrecca, Claudia Innocenti, César de Julián Fernández, Giovanni Bertoni, Clara Marquina, Manuel Ricardo Ibarra, and Claudio Sangregorio**

Supporting Information

3d metal doping of core-shell wüstite@ferrite nanoparticles as promising route towards room temperature exchange bias magnets

Beatrice Muzzi,[a,b,c] Martin Albino,[c] Michele Petrecca,[c] Claudia Innocenti,[b,c] César de Julián Fernández,[d] Giovanni Bertoni,[e] Clara Marquina, [f, g] M. Ricardo Ibarra, [f, g, h] Claudio Sangregorio[b,c]

[a] Dept. of Biotechnology, Chemistry and Pharmacy, University of Siena 1240, I-53100 Siena, Italy

[b] ICCOM - CNR, I-50019 Sesto Fiorentino (FI), Italy

[c] Dept. of Chemistry "U. Schiff", University of Florence and INSTM, I-50019 Sesto Fiorentino (FI), Italy

[d] IMEM - CNR, I-43124 Parma, Italy

[e] CNR – Istituto Nanoscienze, I-41125 Modena, Italy

[f] Instituto de Nanociencia y Materiales de Aragón (INMA), Consejo Superior de Investigaciones Científicas (CSIC)-Universidad de Zaragoza, 50009-Zaragoza, Spain

[g] Dpto. de Física de la Materia Condensada, Universidad de Zaragoza, 50009-Zaragoza, Spain

[h] Laboratorio de Microscopias Avanzadas (LMA), Universidad de Zaragoza, 50018- Zaragoza, Spain

Keywords: core-shell nanoparticles, Néel temperature, doped-wüstite, exchange bias

X-Ray Diffraction (XRD)

The related Powder X-Ray Diffraction measurements, (XRD), reported in Figure S1, confirmed the formation of a rock-salt crystallographic phase, corresponding to the space group $\boldsymbol{Fm\bar{3}m}$ (*JCPDS PDF #73-2144*), for the three samples. Moreover, the peak at 2θ = 36°, corresponding to the (311) main peak of the cubic spinel structure (space group $\boldsymbol{Fd\bar{3}m}$, *JCPDS PDF #19-0629*), suggests the presence of a very thin shell of ferrite. This feature is better appreciated in the **FeO** sample, probably due to a thicker shell. The shell formation arises from the controlled oxidation and passivation of the monoxide particles, during the cleaning procedure, which was also exploited for the magnetic separation of the nanoparticles from the reaction media.

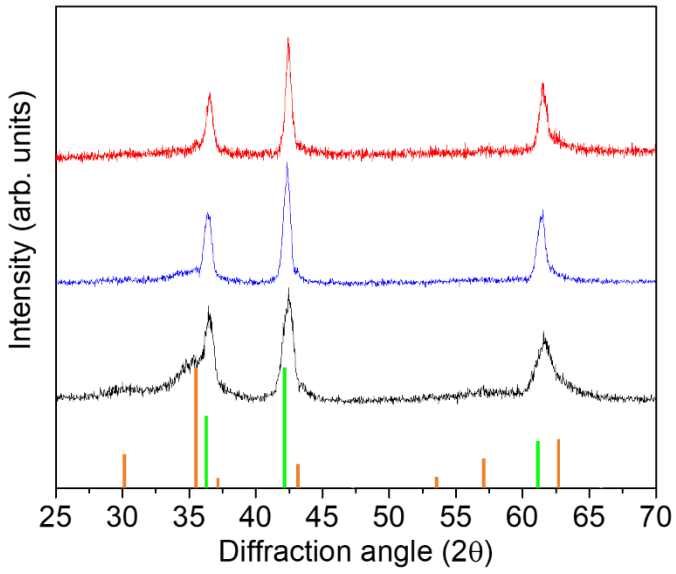

Figure S1. Experimental XRD patterns of the three samples: **FeO** (black line), **CoFeO** (blue line), **NiCoFeO** (red line) and the reference patterns: $Fe_{1-x}O$ (*JCPDS PDF #73-2144*) and Fe_3O_4 (*JCPDS PDF #19-0629*).

High Resolution Transmission Electron Microscopy (HRTEM)

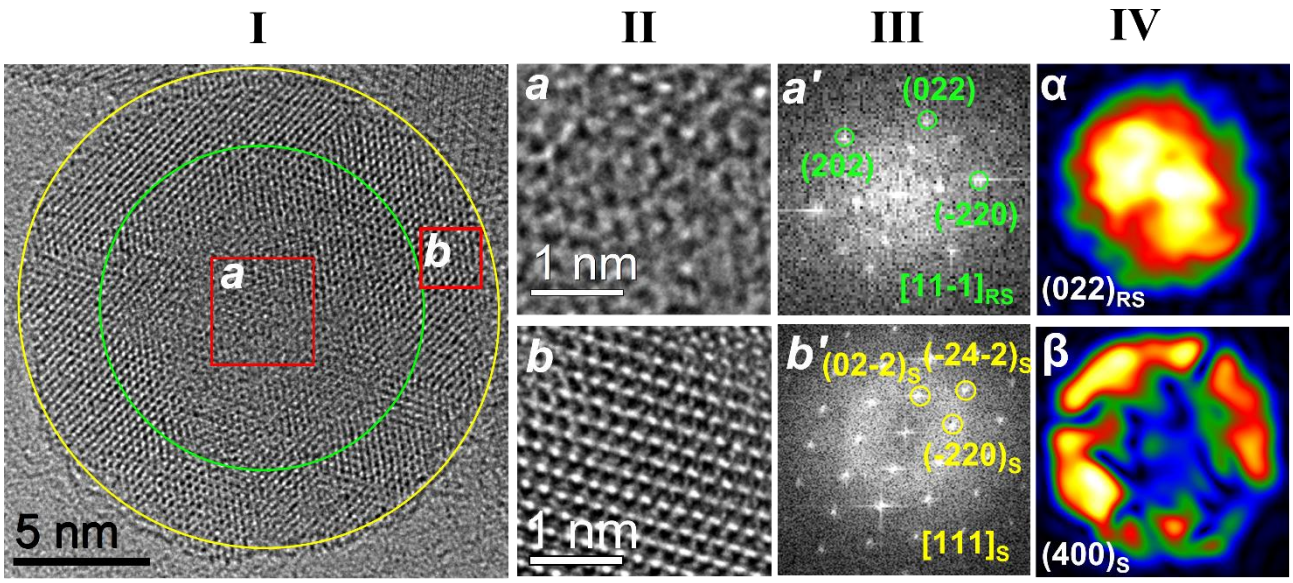

Figure S2. (I) HRTEM image of a **FeO** NP, where 2 regions (red squares *a* and *b*) are selected: *a* and *b* correspond to $Fe_{0.95}O$ rock-salt core and Fe_3O_4 spinel ferrite shell, respectively. (II) Enlargement of the selected regions. (III) FFT analysis of the two regions showing the presence of different crystallographic structures; the labelled spots are related to crystallographic planes that can be indexed as: *a'*) rock-salt phase ($\boldsymbol{Fm\bar{3}m}$), in zone axis $[11\text{-}1]_{RS}$, and *b'*) cubic spinel structure ($\boldsymbol{Fd\bar{3}m}$), $[111]_S$. (IV) Geometrical Phase Analysis of the same NP: the yellow and red colours indicate the presence and the localization within the NP of the crystallographic directions taken into account, which are the $(022)_{RS}$ and $(400)_S$, related to the rock-salt (α) and the spinel (β), respectively.

To exclude the oxidation of magnetite (Fe_3O_4) to maghemite (γ-Fe_2O_3) under air exposition, the Fe_3O_4 lattice parameter was determined from the positions of the reflections in the reciprocal space (figure S2b') obtained from the FFT of the **FeO** HRTEM image. By the equation $1/d^2 = (h^2+k^2+l^2)/a^2$, where d is the value of the unit cell parameter in the reciprocal space, (hkl) are the Miller's indexes and a is the lattice parameter in the real space, the calculated a = 8.41 Å, confirmed the formation of Fe_3O_4 as shell (Fe_3O_{4bulk} = 8.39 Å and γ-Fe_2O_{3bulk} = 8.33 Å)[1,2] and underlined the stability of Fe_3O_4 phase to oxidation process during long exposure time. This result was also confirmed by the quantification of the two EELS spectra (core and shell) after principal component

analysis (PCA) decomposition (Figure S4). The extracted Fe/O atomic ratio confirmed the formation of Fe_3O_4 shell with respect to the more oxidized γ-Fe_2O_3 phase:

shell: Fe/O = 0.77± 0.04 (for Fe_3O_4 expected at 0.75, while for γ-Fe_2O_3 is expected at 0.67).

core: Fe/O = 0.86± 0.04 ($Fe_{1-x}O$ expected close to 1.0; the experimental value is possibly lower because for the core region we have the additional contribution from the shell at the top and at the bottom).

For a statistical analysis, these treatments were performed on ca. 10 **FeO** NPS.

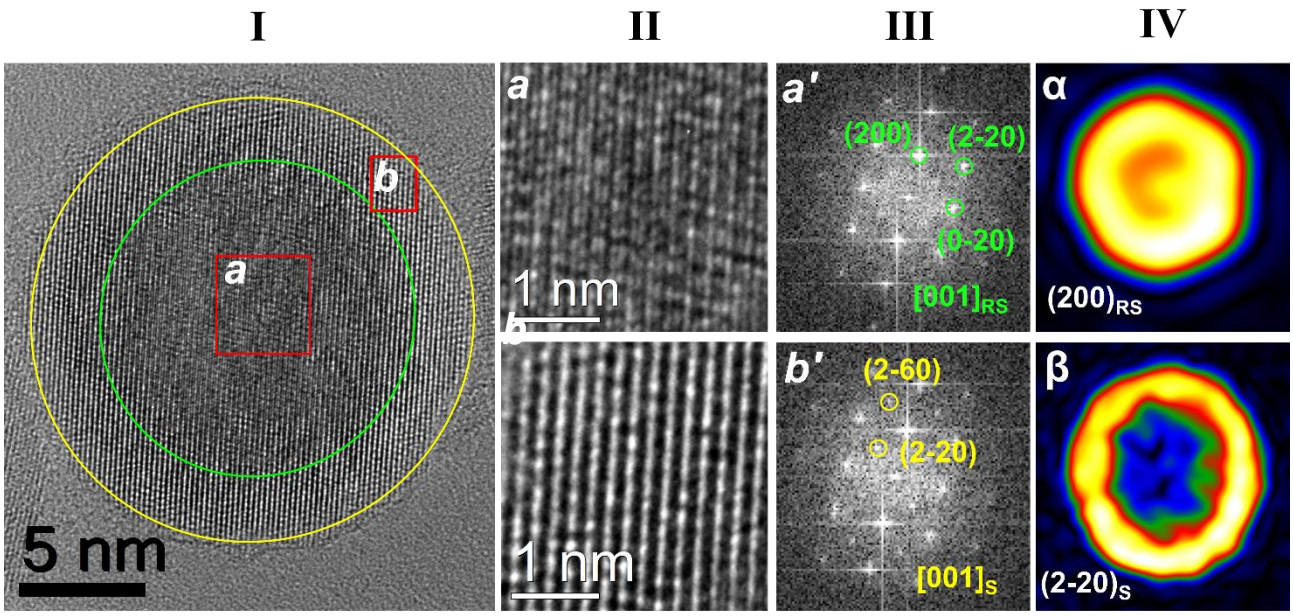

Figure S3. (I) HRTEM image of a **CoFeO** NP, where 2 regions (red squares *a* and *b*) are selected: *a* and *b* correspond to $Co_{0.3}Fe_{0.7}O$ rock-salt core and $Co_{0.8}Fe_{2.2}O$ spinel ferrite shell, respectively. (II) Enlargement of the selected regions. (III) FFT analysis of the two regions showing the presence of different crystallographic structure; the labelled spots are related to crystallographic planes that can be indexed as: *a'*) rock-salt phase ($\boldsymbol{Fm\bar{3}m}$), in zone axis $[001]_{RS}$, and *b'*) cubic spinel structure ($\boldsymbol{Fd\bar{3}m}$), $[001]_S$. (IV) Geometrical Phase Analysis of the same NP: the yellow and red colours indicate the presence and the localization within the NP of the $(200)_{RS}$, α, and $(2\text{-}20)_S$, β, crystallographic directions, which are related to the rock-salt and the spinel, respectively

Electron Energy Loss Spectroscopy (EELS) analysis

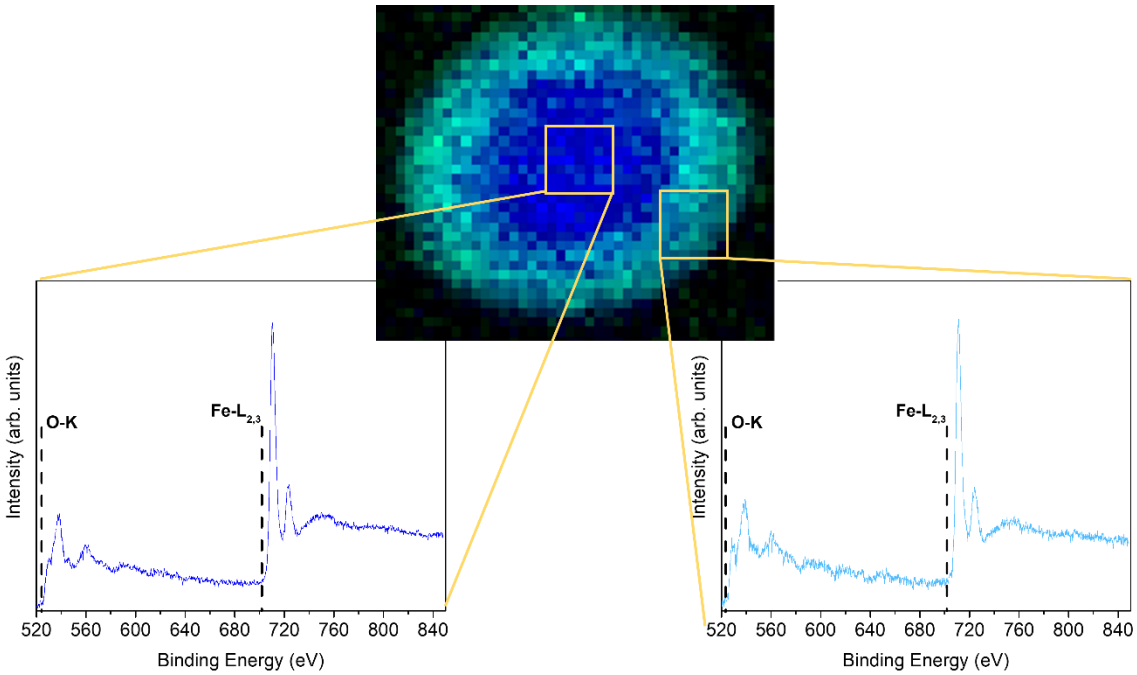

Figure S4. STEM image of a **FeO** NP and EELS spectra of the core and shell regions obtained by PCA decomposition.[3] Peaks corresponding to oxygen (O-K edge) and iron (Fe-$L_{2,3}$) are shown in the EELs spectra.

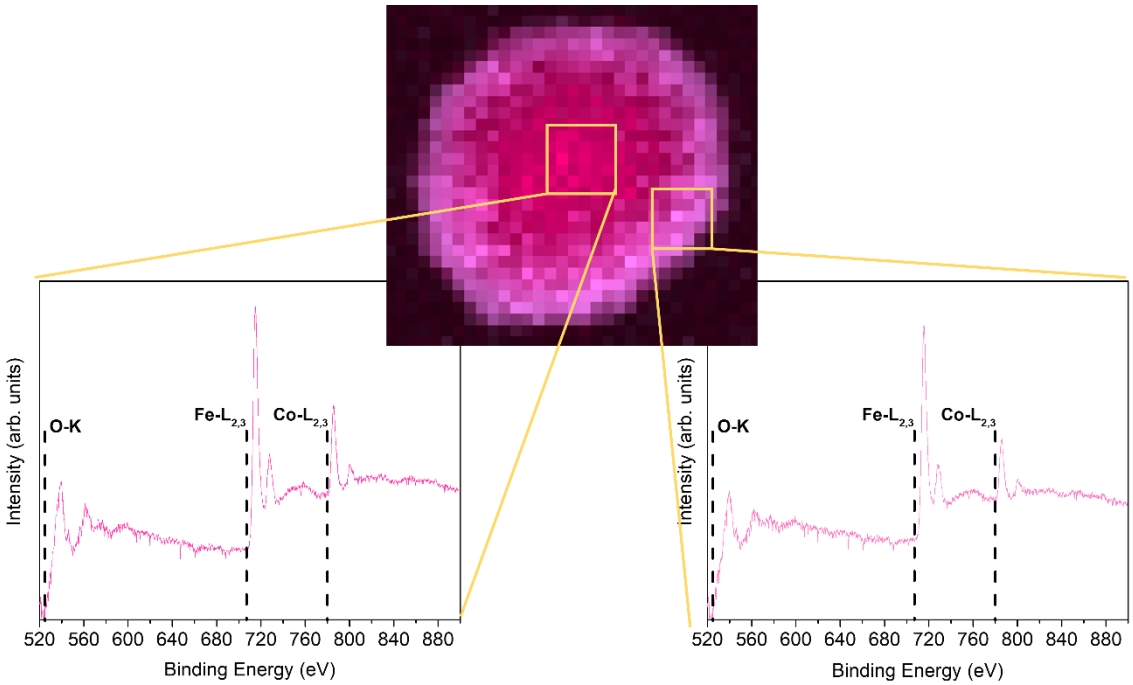

Figure S5. STEM image of a **FeO** NP and EELS spectra of the core and shell regions obtained by PCA decomposition.[3] Peaks corresponding to oxygen (O-K edge), iron (Fe-$L_{2,3}$) and cobalt (Co-$L_{2,3}$) are shown in the EELs spectra.

Energy Dispersive X-Ray Fluorescence (EDXRF)

Table S1. Iron, cobalt and nickel atomic percentage obtained by Energy Dispersive X-Ray Fluorescence (EDXRF) for **CoFeO** and **NiCoFeO.**

Samples	Fe (atomic %)	Co (atomic %)	Ni (atomic %)
CoFeO	69	31	-
NiCoFeO	64	17	19

Magnetic measurements

The hysteresis loops at 5 K representative of the FiM shell in the three samples (Figure S6) were obtained by the subtraction of the AFM contribution extrapolated by a linear fit of the 5 K loops at high magnetic field (M = χ^{AFM} H). The susceptibility (χ^{AFM}) related to the monoxide core for the

iron and doped monoxides NPs, were obtained by the M/H ratio at high field and are reported in Table S2. After the removal of the AFM linear contribution the higher $\mu_0 H_c^{FiM}$ value for **CoFeO** is in agreement with the large amount of $Co^{(II)}$ in the lattice, which increases the magnetic anisotropy of the NPs. While the **CoFeO** loop maintains a strong AFM-like character, the **NiCoFeO** becomes much more ferrimagnetic-like, with a greater squareness and remanence value, suggesting that the $Ni^{(II)}$ induces a recovery of the magnetic order in the shell respect to **CoFeO**. Concerning the magnetization at 5 T (M_{5T}^{FiM}) reported in Table S2, the highest M_{5T}^{FiM} value is obtained for **FeO** and this result can be ascribed to the more ordered and thicker ferrite shell on the wüstite core, confirming the HRTEM data analysis reported above.

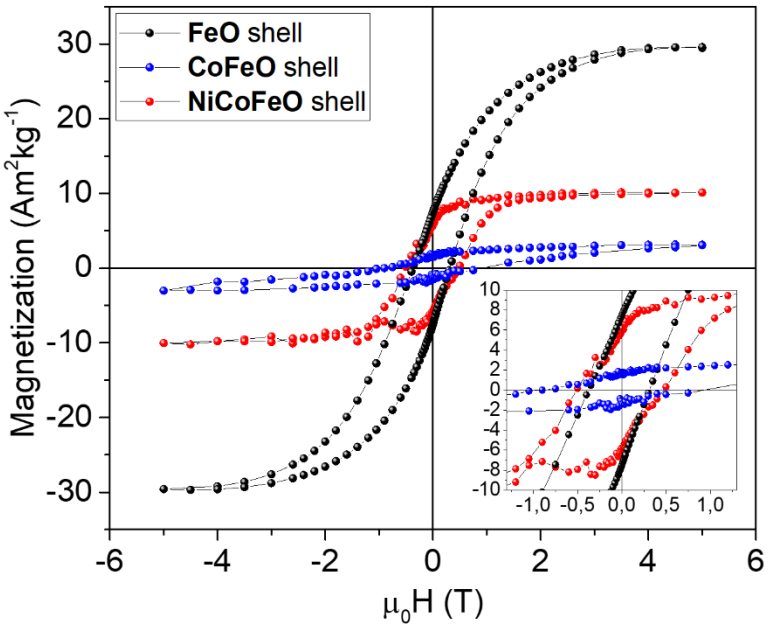

Figure S6. Magnetization loops of the FiM shell component for the 3 samples at 5 K.

Table S2. Magnetization at 5 T, M_{5T}; remanence, M_R (reduced remanence R% in brackets) and coercive field, $\mu_0 H_C$ at 5 K for FiM phase in **FeO**, **CoFeO** and **NiCoFeO**. The magnetization values are normalized to the weight of the total inorganic component.

Sample	5 K			
	M_{5T}^{FiM} (Am^2kg^{-1})	M_R (R%) (Am^2kg^{-1})	$\mu_0 H_C^{FiM}$ (T)	χ^{AFM} (Am^2kg^{-1})
FeO	30	8 (27)	0.38	$2.33*10^{-4}$
CoFeO	3	1.7 (57)	0.90	$1.54*10^{-4}$
NiCoFeO	10	6 (60)	0.51	$1.10*10^{-4}$

To reduce the minor loop effect on the vertical shift of the **CoFeO** hysteresis, four loops at 5 K after FC procedure applying 3 T, 5 T, 7 T and 12 T, were recorded. In Figure S7 a, a progressive vertical symmetrization (M_{VS}) of the loop by increasing the intensity of the applied field is shown (see also M_{VS} in Figure S7 b), even if the irreversibility persists up to 12 T. Both $\mu_0 H_C^{FC}$ and $\mu_0 H_E$ (Figure S7 b) tend to stabilize with increasing fields, as expected when magnetic saturation is approaching. While $\mu_0 H_C^{FC}$ follows the increase of the FC field, corresponding to the maximum field of the cycle, $\mu_0 H_E$ value decreases to 0.76 T when the vertical shift is minimized, confirming that this is mainly due to the minor loop effect rather than to the spin pinning at the interface.

Even if the AFM-like contribution is lower, a similar behavior was also observed for **NiCoFeO**. In Figure S7 c, indeed, a progressive vertical symmetrization is shown when the intensity of the applied FC field is increased from 3 to 9 T.

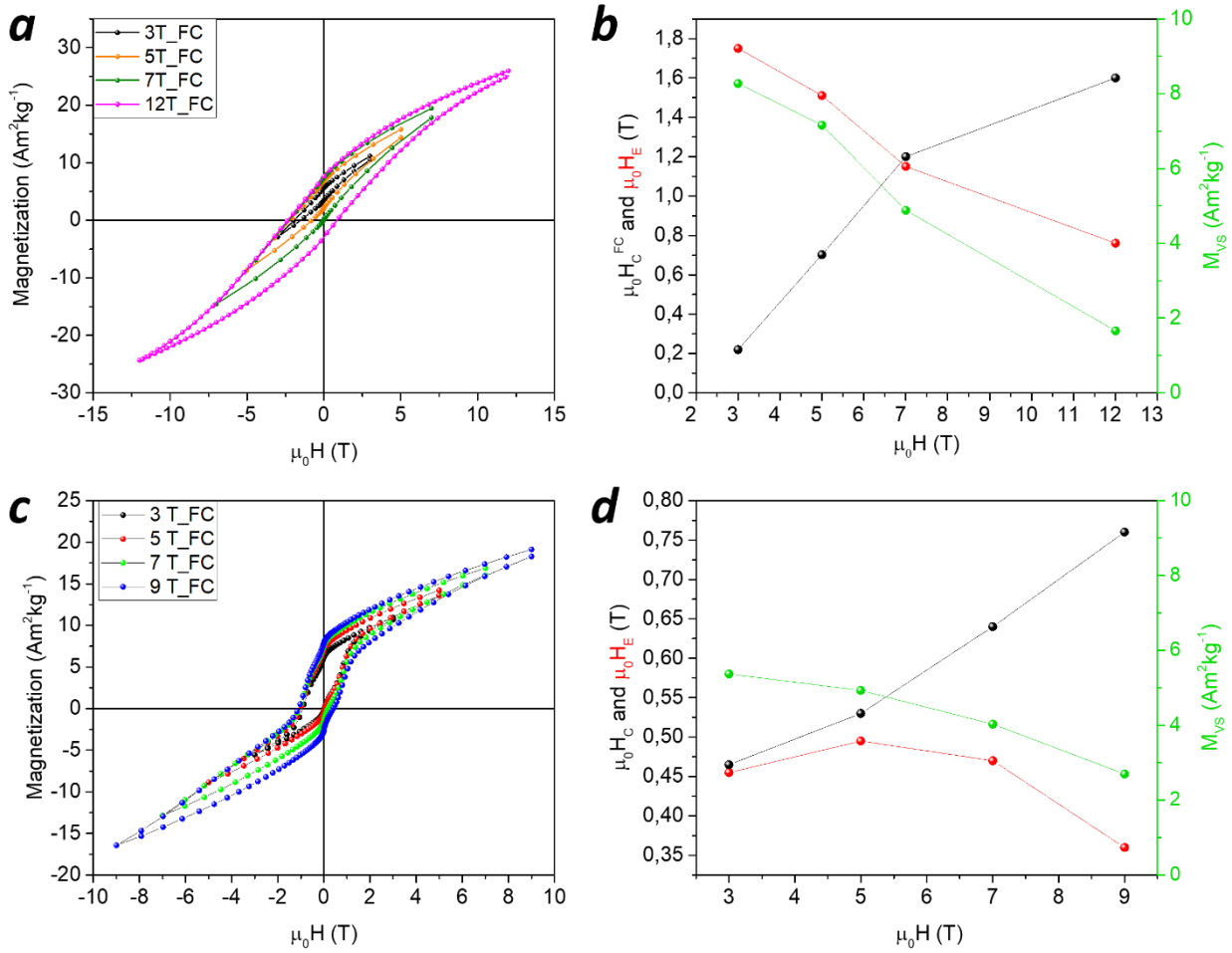

Figure S7. *a*) hysteresis loops of sample **CoFeO** recorded after FC procedure applying 3 T (black line), 5 T (orange line), 7 T (green line) and 12 T (magenta line); *b*) recorded coercive field ($\mu_0 H_C^{FC}$), exchange bias field ($\mu_0 H_E$) and vertical shift ($M_{vs} = (M_{5T}^{+} - M_{5T}^{-})/2)$) as a function of the applied field during the FC process; *c*) hysteresis loops of sample **NiCoFeO** recorded after FC procedure applying 3 T (black line), 5 T (red line), 7 T (green line) and 9 T (blue line); *d*) recorded coercive field ($\mu_0 H_C^{FC}$), exchange bias field ($\mu_0 H_E$) and vertical shift as a function of the applied field during the FC process.

XRD and Magnetic properties of $Ni_{0.18}Co_{0.22}Fe_{0.60}O@Ni_{0.5}Co_{0.7}Fe_{1.8}O_4$ nanoparticles

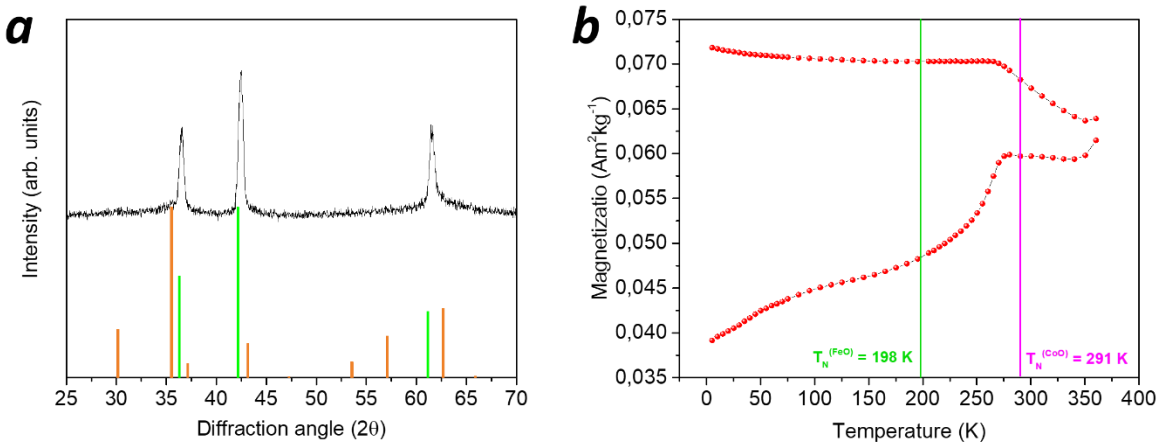

Figure S8. *a)* Experimental XRD patterns of the $Ni_{0.18}Co_{0.22}Fe_{0.60}O@Ni_{0.5}Co_{0.7}Fe_{1.8}O_4$ and the reference patterns: $Fe_{1-x}O$ (*JCPDS PDF #73-2144*) and Fe_3O_4 (*JCPDS PDF #19-0629*); *b)* Temperature dependence of the magnetization recorded after ZFC and FC procedures, applying a static field of 5 mT

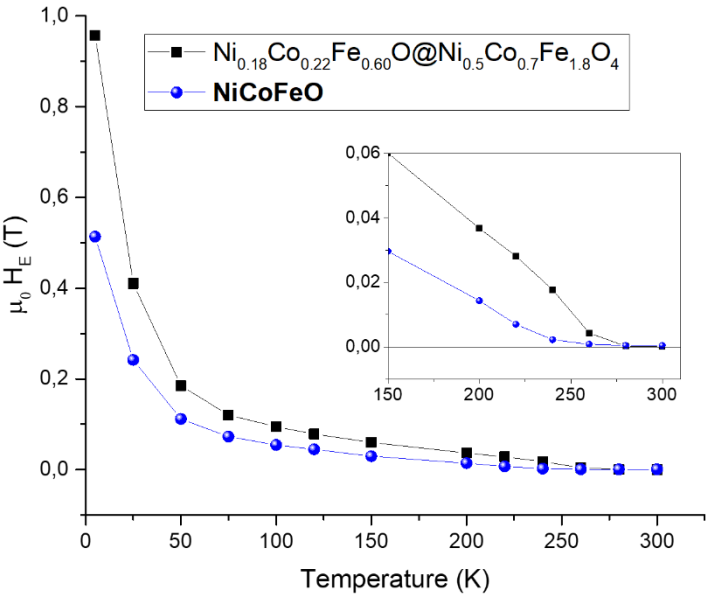

Figure S9. Exchange bias field ($\mu_0 H_E$) as a function of the temperature at which the hysteresis loop has been recorded after the FC 5T process for **NiCoFeO** and $Ni_{0.18}Co_{0.22}Fe_{0.60}O@Ni_{0.5}Co_{0.7}Fe_{1.8}O_4$.

References

[1] C. Pecharromán, J. E. Gonzalez-Carreno, T., Iglesias, *Phys. Chem. Miner.* **1995**, *22*, 21.

[2] H. S. C. O'Neill, W. A. Dollase, *Phys. Chem. Miner.* **1994**, *20*, 541.

[3] G. Lucas, P. Burdet, M. Cantoni, C. Hébert, *Micron* **2013,** *52-53,* 49.